HeartRhythm

The Official Journal of the Heart Rhythm Society, The Cardiac Electrophysiology Society, and The Pediatric & Congenital Electrophysiology Society

Heart Rhythm Society SM

Creative Concepts

Check for updates

The right atrium affects *in silico* arrhythmia vulnerability in both atria

Patricia Martínez Díaz, MSc,[1] Jorge Sánchez, PhD,[2] Nikola Fitzen, BSc,[1] Ursula Ravens, MD, PhD,[3] Olaf Dössel, PhD,[1] Axel Loewe, PhD[1]

KEYWORDS Atrial fibrillation; Right atrium; Arrhythmia vulnerability; Personalized computer model; Atrial remodeling; Computer simulation

(Heart Rhythm 2024;21:799–805)

Introduction

The role of the right atrium (RA) in atrial fibrillation (AF) has long been overlooked. Multiple studies have examined clinical conditions associated with AF, such as atrial enlargement, fibrosis extent, electrical remodeling, and wall thickening, but have been mainly concentrated on the left atrium (LA). AF research predominantly focuses on the LA because of 2 key paradigms. First, the well-established view that AF onset is primarily triggered by activity originating in the pulmonary veins of the LA.[1] Second, comorbidities linked to AF, such as hypertension, valvular disease, and heart failure, primarily impact the left side of the heart, contributing to increased mortality and reduced quality of life. Thus, AF research continues to focus mostly on the LA, and, as a consequence, the role of the RA in AF is barely understood.

With the advent of personalized medicine, patient-specific computer models of the atria are enhancing our understanding of intricate interactions during AF and have already been used to identify ablation targets, tailor ablation strategies, and predict recurrence in AF patients.[2–5] Nevertheless, those methodologies did not specifically focus on the role of the RA, with some excluding RA tissue and others neglecting the assessment of AF induction or maintenance from RA sources.

Computer models of the atria can aid in assessing how the RA influences arrhythmia vulnerability and in studying the role of RA drivers in the induction of AF, both aspects difficult to assess clinically and experimentally. This work assesses the "Creative Concept" of incorporating the RA in computational arrhythmia studies based on 1398 virtual pacing sequences in 8 biatrial and 8 monoatrial patient-specific models under 3 different substrate conditions, resulting in a total of 48 distinct model configurations.

Methods

A general overview of the study methodology is shown in Figure 1.

Patient-specific anatomic modeling

Imaging data from 8 subjects (P1–P8) were obtained as described previously[6] and used to generate the biatrial personalized anatomic models. Subjects provided written informed consent, and the study protocol was reviewed and approved by the ethical committee of Guy's Hospital, London, United Kingdom, and University Hospital Heidelberg, Heidelberg, Germany. The research reported in this article adhered to the Helsinki Declaration guidelines.

The cohort characteristics are given in Supplemental Table S1. Patient-specific bilayer models were generated following the methodology described by Azzolin et al.[7] For each subject, we created 2 models: (1) *monoatrial* with only the LA; and (2) *biatrial* with both the RA and LA. Using rule-based definitions,[8] 4 interatrial connections (IACs) were added automatically to the biatrial models: a middle posterior bridge, an upper posterior bridge, Bachmann bundle, and 1 via the coronary sinus. Further details on interatrial connection (IAC) modeling are shown in Supplemental Figure S1. Cellular electrophysiology of atrial myocytes was modeled using the mathematical model of Courtemanche et al.[9] To compute electrical propagation in the human atria, we solved the monodomain equation using the electrophysiology

From the [1]Institute of Biomedical Engineering, Karlsruhe Institute of Technology (KIT), Karlsruhe, Germany, [2]Institute of Information and Communication Technologies (ITACA), Universitat Politècnica de València (UPV), Valencia, Spain, and [3]Institute for Experimental Cardiovascular Medicine, Universitätsklinikum Freiburg, Freiburg, Germany.

https://doi.org/10.1016/j.hrthm.2024.01.047

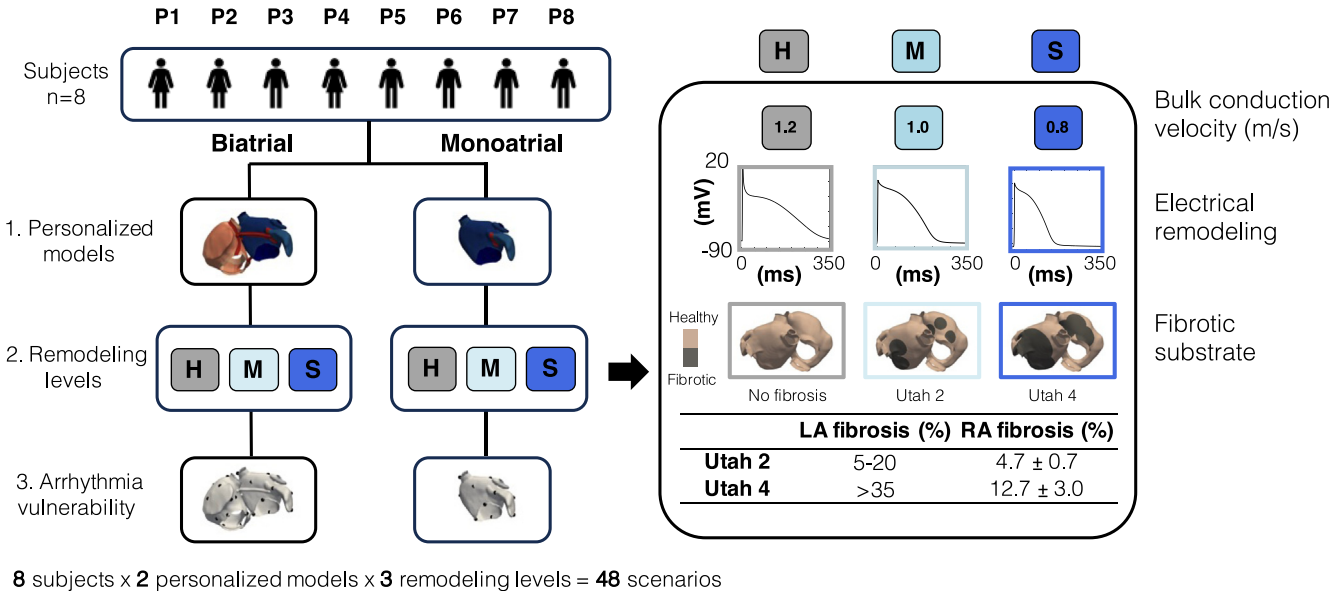

Figure 1
Study methodology. **Left:** Virtual cohort generation considering biatrial and monoatrial configurations with 3 remodeling levels to assess arrhythmia vulnerability. **Right:** Fibrotic substrate modeling approach considering changes in conduction velocity, electrical remodeling, and fibrosis extent (H = healthy; M = mild; S = severe). LA = left atrium; RA = right atrium.

simulator openCARP.[10,11] Both the carputils bundle containing the openCARP experiment, along with all associated parameters,[12] and the dataset with the biatrial and monoatrial models[13] are publicly available.

Electrophysiological modeling

We defined 3 different levels of AF-induced remodeling—healthy (H), mild (M), and severe (S)—by reducing the conductance of a set of ionic channels in the model of Courtemanche et al as described previously,[14] with 0%, 50%, and 100% changes for H, M, and S, respectively. The maximum scaling of the ionic conductances affects the action potential in line with the changes observed in human atrial myocytes in patients with persistent AF.[15] The scaling factors applied to the ionic conductances and their corresponding action potential features are detailed in Supplemental Table S2. Mean conduction velocity (CV) of 1.0 m/s was reported in patients with persistent AF.[16] To consider the 3 remodeling states, we introduced a 20% variation in CV. The models were parameterized to yield a CV along the myocyte preferential direction of 1.2, 1.0, and 0.8 m/s for each remodeling level, respectively. Intracellular and extracellular conductivities were scaled $\times 3$ for the Bachmann bundle and $\times 2$ for the crista terminalis and pectinate muscles with respect to normal myocardium. Regional ionic heterogeneity and anisotropy ratios are detailed in Supplemental Table S3.[17,18]

Fibrotic substrate modeling

The fibrotic substrate was modeled based on Nagel et al.[19] (Supplemental Figure S2). Fibrosis extent corresponded to Utah stage 2 (5%–20%) and Utah stage 4 (>35%) for the M and S states, whereas the H state was modeled without fibrosis. The proportion of RA and LA fibrosis extent was based on the percentages reported by Akoum et al.[20] To consider the multifactorial nature of fibrosis, we modeled fibrotic regions with 30% of the elements as nonconductive, with $\sigma = 10^{-7}$ S/m to account for electrical myocyte decoupling, and the rest affected by transforming growth factor β1–induced electrical remodeling in response to cellular inflammation.[21,22]

Arrhythmia vulnerability

Arrhythmia vulnerability was assessed by an S1-S2 pacing protocol with 2-cm interpoint distance on the atrial surface.[23] Stimulation points and earliest activation sites on the LA remained consistent between monoatrial and biatrial configurations. A point was classified as inducing if reentry was maintained for at least 1 second. The vulnerability ratio was defined as the number of inducing points divided by the number of stimulation points. Mean tachycardia cycle length (TCL) of the induced reentries was assessed at the stimulation site (Supplemental Figure S3).

Statistical analysis

Data are given as mean ± SD. To evaluate statistical significance between the sample means, we conducted a 2-sampled t-test. $P < .05$ was considered significant.

Results

The 8 biatrial anatomic models and the number of stimulation points in each chamber are shown in Figure 2. The amount of fibrosis for each subject in each stage is given in Supplemental Table S4.

A **Patient-specific biatrial models derived from CT and MR segmentations**

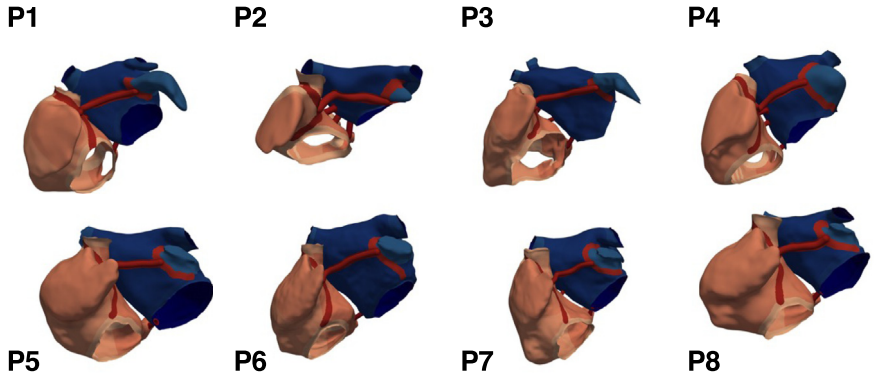

B **Stimulation points for the vulnerability protocol**

Subject	LA	RA	Total
P1	14	17	26
P2	7	10	17
P3	18	24	39
P4	18	19	37
P5	24	29	54
P6	23	21	40
P7	29	32	61
P8	15	18	31

Figure 2
Personalized models (**A**) and total number of stimulation points used to assess arrhythmia vulnerability (**B**). CT = computed tomography; LA = left atrium; MR = magnetic resonance; RA = right atrium.

Vulnerability of the LA in monoatrial and biatrial configurations

We ran 444 monoatrial simulations, from a total of 148 stimulation points × 3 remodeling states in the 8 LA models, and 954 biatrial simulations, from a total of 318 stimulation points × 3 remodeling states in the 8 biatrial models to assess arrhythmia vulnerability. The number of inducing points and the vulnerability ratio V_{LA} for each subject in each configuration are shown in Figure 3.

A total of 79 reentry episodes were induced in the monoatrial configuration, of which 32 episodes were in the M state and 47 in the S state. No reentries were induced in the H state. In the biatrial configuration, a total of 281 reentry episodes were induced, of which 130 were induced by pacing from the LA. In the H state, only 1 reentry was induced by pacing from the LA anterior wall in proximity to the mitral valve in P6.

The monoatrial vulnerability ratio V_{LA} among all subjects in the M and S states was 0.19 ± 0.13 and 0.31 ± 0.14, respectively. The biatrial vulnerability ratio V_{LA} between the M and S states showed minimal changes (0.41 ± 0.22 vs 0.40 ± 0.15, respectively). Incorporating the RA increased in mean V_{LA} vulnerability by 115.8% in the M state and by 29.0% in the S state (Figure 4A).

In the monoatrial configuration, there was a 20.0% increase in mean TCL between states M and S (186.94 ± 13.3 ms vs 224.32 ± 27.6 ms; P <.001). While in the biatrial configuration, mean TCL of LA-induced reentries showed a 5.6% increase between the M and S states (197.24 ± 18.3 ms vs 208.24 ± 34.8 ms; P = .026). Including the RA led to changes in mean TCL of the LA-induced reentries by 5.5% (P = .006) in the M scenario and a decrease of 7.2% (P = .010) in the scenario S (Figure 4B).

Increased remodeling from M to S in the monoatrial configuration revealed 4.3 ± 2.9 new inducing points in the LA per patient (Figure 5A). The points became inducing when going from M to S due to rotational activity near the fibrotic regions.

A **Monoatrial**

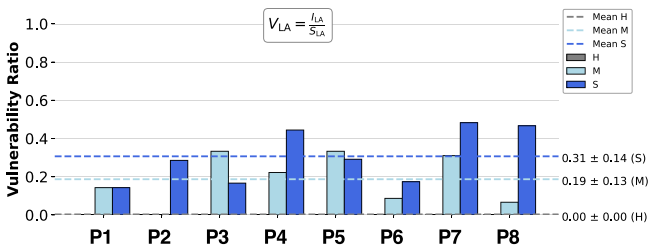

	P1	P2	P3	P4	P5	P6	P7	P8	
	LA	LA	LA	LA	LA	LA	LA	LA	**Total**
SP	14	7	18	18	24	23	29	15	**148**
I_H	0	0	0	0	0	0	0	0	**0**
I_M	2	0	6	4	8	2	9	1	**32**
I_S	2	2	3	8	7	4	14	7	**47**

B **Biatrial**

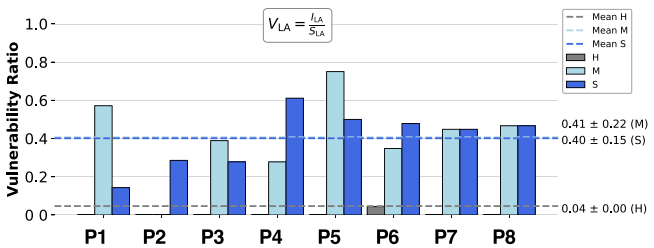

	P1		P2		P3		P4		P5		P6		P7		P8		
	LA	RA	LA	RA	LA	RA	LA	RA	LA	RA	LA	RA	LA	RA	LA	RA	**Total**
SP	14	17	7	10	18	24	18	19	24	29	23	21	29	32	15	18	**318**
I_H	0	0	0	0	0	0	0	0	0	0	1	0	0	0	0	0	**1**
I_M	8	4	0	0	7	9	5	0	18	12	8	10	13	12	7	5	**118**
I_S	2	16	2	4	5	9	11	11	12	20	11	13	13	19	7	7	**162**

Figure 3
Vulnerability of the left atrium (LA) in monoatrial (**A**) and biatrial (**B**) configurations. *Dashed lines* represent mean vulnerability ratios for each remodeling level. I_{LA} = inducing points in the left atrium; I_H, I_M, I_S = inducing points in each remodeling level (H = healthy; M = mild; S = severe); SP = stimulation point.

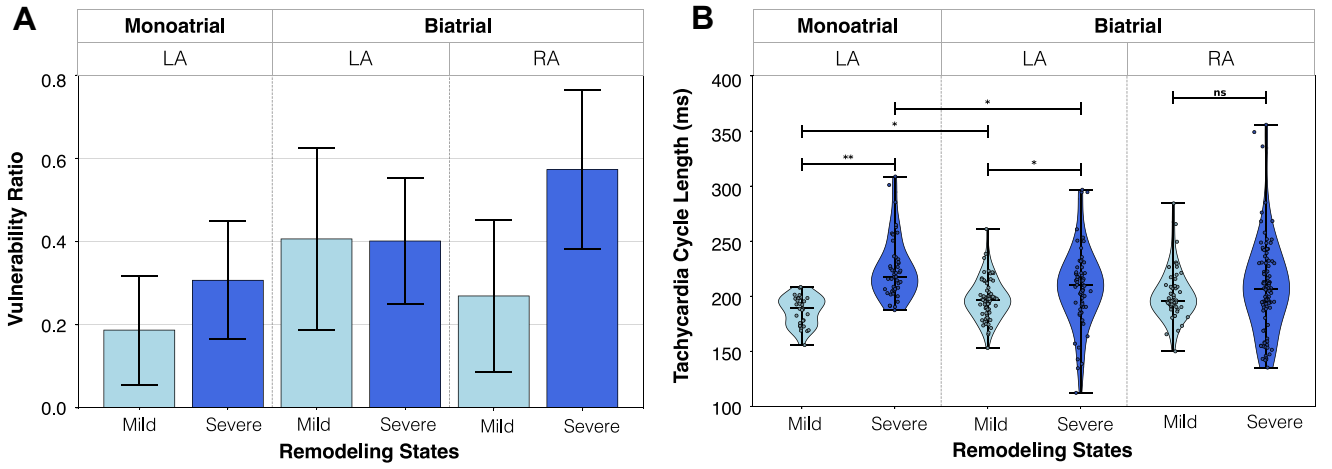

Figure 4
Impact of the right atrium (RA) on arrhythmia vulnerability ratio (**A**) and tachycardia cycle length (**B**). *Bars* depict vulnerability ratios, calculated as the number of induced points to the total points in each chamber across all 8 subject models. *Violin plots* show the probability density of tachycardia cycle length measurements, with scatter points representing each reentry measurement. **P* <.05; ***P* <.001; ns = not significant.

Deceleration of the wavefront and a shortened action potential in S enabled propagation within the fibrotic region. In contrast, in M, the faster wavefront encountered refractory tissue and failed to activate the surrounding tissue.

To assess the role of the RA on LA inducibility in greater detail, we evaluated changes in LA inducibility by comparing points within the LA initiating reentry with and without the RA (Figure 5B). Inclusion of the RA resulted in elevated LA inducibility, uncovering 5.5 ± 3.0 inducing points in the LA biatrial scenarios that did not induce in the monoatrial configuration (Figure 6). The IACs contributed to the increased reentry inducibility (Figure 7).

Vulnerability of the RA

A total of 151 of 281 biatrial reentry episodes were induced by pacing from the RA. The vulnerability ratio of the RA (V_{RA}) showed a 111.1% increase between states M and S (0.27 ± 0.18 vs 0.57 ± 0.19) (Figure 4A). Mean TCL of the RA-induced reentries for the M and S state was 201.33 ± 23.0 ms and

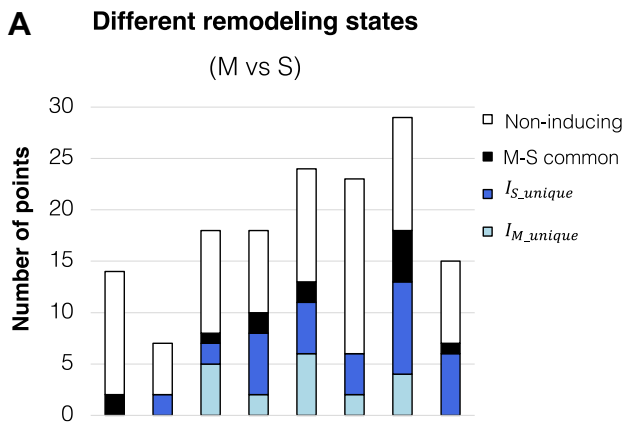

	P1	P2	P3	P4	P5	P6	P7	P8	Mean ± SD
I_{M_total}	2	0	6	4	8	2	9	1	**4.0 ± 3.3**
I_{S_total}	2	2	3	8	7	4	14	7	**5.9 ± 4.1**
I_{M_unique}	0	0	5	2	6	2	4	0	**2.4 ± 2.4**
I_{S_unique}	0	2	2	6	5	4	9	6	**4.3 ± 1.9**
I_{common}	2	0	1	2	2	0	5	1	**1.6 ± 1.6**
N_{common}	12	5	10	8	11	17	11	8	**10.3 ± 3.5**

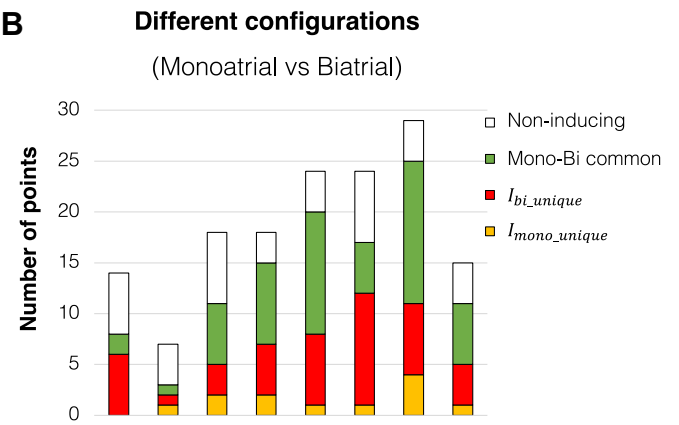

	P1	P2	P3	P4	P5	P6	P7	P8	Mean ± SD
I_{mono_total}	2	2	8	10	13	6	18	7	**8.3 ± 5.4**
I_{bi_total}	8	2	9	13	19	16	21	10	**12.3 ± 6.3**
I_{mono_unique}	0	1	2	2	1	1	4	1	**1.5 ± 1.2**
I_{bi_unique}	6	1	3	5	7	11	7	4	**5.5 ± 3.0**
I_{common}	2	1	6	8	12	5	14	6	**6.8 ± 4.5**
N_{common}	6	4	7	3	4	7	4	4	**4.9 ± 1.6**

Figure 5
Proportion of inducing (I) and noninducing (N) points in the left atrium is higher with increased remodeling in the monoatrial configuration (**A**) and with incorporation of the right atrium in biatrial configuration (**B**). Unique refers to points that exclusively induce in a specific setup. Bi = biatrial; M = mild; S = severe.

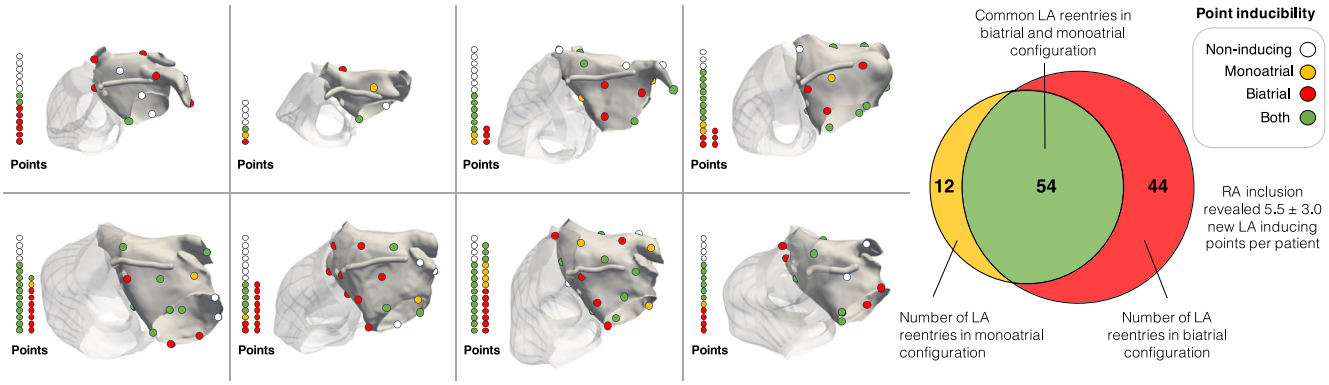

Figure 6
Increased left atrium (LA) inducibility due to right atrium (RA) incorporation. Meshes display LA stimulation points inducing reentry in monoatrial *(yellow)*, biatrial *(red)*, and both *(green)* configurations, or noninducing *(white)*. *Columns* represent the inducibility type at each stimulation point. The Venn diagram (**right**) depicts monoatrial and biatrial reentry distribution among all subjects.

207.87 ± 41.6 ms, respectively (P = .295) (Figure 4B). The biatrial vulnerability (V_{Bi}) including both the RA and LA is shown in Supplemental Figure S4.

Discussion

This study assessed 48 arrhythmia vulnerability scenarios in 8 patient-specific anatomic models considering monoatrial and biatrial configurations and 3 remodeling states (H, M, and S). The main focus was to assess the role of the RA in arrhythmia vulnerability.

Impact of the RA

The notion that the RA could play a role in AF is not a novel concept, as indicated by Nitta et al.[24] However, the existing literature often neglects this potential role and provides limited evidence regarding the extent to which the RA contributes to the initiation and maintenance of AF. The term "right atrium" is scarcely mentioned in the latest guidelines for AF treatment.[25,26] This highlights a lack of comprehensive studies investigating the role of the RA in the context of AF prevention and treatment.

Among all investigated configurations, the RA was the chamber with the highest vulnerability in the S state. A possible explanation could be the larger RA size and the increased electrophysiological heterogeneity due to the presence of the pectinate muscles, crista terminalis, and tricuspid valve. Despite the lower fibrotic extent in the RA compared to the LA, the RA was more vulnerable to developing reentry upon stimulation than the LA.

We identified additional inducing points in the LA biatrial configuration that did not induce reentry in the LA-only model (Figure 7). IACs can promote reentrant circuits and facilitate arrhythmia maintenance, as shown by Roney et al.[27] Furthermore, for reentry to occur, an excitable gap is crucial, requiring the wavelength to be shorter than the reentrant circuit length. As a result, incorporating the RA increases the likelihood of new reentrant circuits influenced not only by larger size but also by changes in the wavelength due to regional differences in CV and effective refractory period.[18]

Previous computational model studies have established that the dynamics of reentrant drivers are influenced by the extent and distribution of the fibrotic substrate, in the RA[28] and the LA.[29] Moreover, investigations by Boyle et al.[2] and Zahid et al.[28] have identified reentrant drivers in the RA through the utilization of biatrial models. We also observed simultaneous interactions of multiple reentries (functional and anatomic) in the biatrial simulations, such as rotational activity around the atrioventricular valves, unidirectional blocks in the Bachmann bundle region, reentrant pathways aided

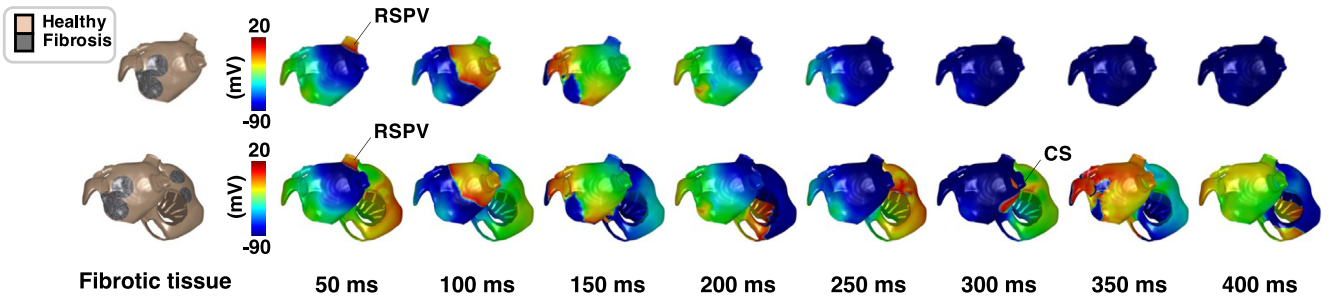

Figure 7
Reentry induction in biatrial configuration aided by interatrial connections involving the posterior wall of the left atrium. The stimulation point at the right superior pulmonary vein (RSPV) of the left atrium initiates the reentrant pathway through the interatrial connections, via the coronary sinus and middle posterior bridge, unsupported by the monoatrial setup.

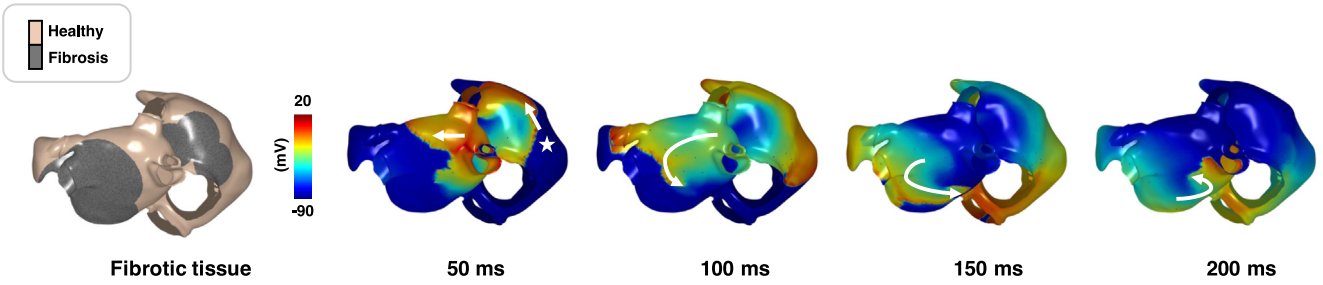

Figure 8
Example of reentry induction from stimulation point in the right atrium in the S state. The inducing point *(star)* is located in the right atrium near the inferior vena cava. The reentry is anchored at the inferior wall of the left atrium, and wave propagation slows down at the border of the fibrotic region.

by IACs, and rotors associated with the fibrotic substrate. We propose that the increased inducibility in the LA biatrial model (ie, additional reentrant drivers) resulted from the interplay between fibrosis characteristics and novel circuit paths (Figure 8).

Incorporating the RA had an impact on LA vulnerability and TCL distribution. Without the RA, the vulnerability of the LA was markedly higher in the S than in the M state. Incorporating the RA notably diminished this difference in LA vulnerability. Adding the RA led to 5.5% slower LA reentries in the M state but 7.2% faster LA reentries in the S state, indicating a state-dependent influence of the RA on reentry dynamics in the LA. The similar TCL between the LA and RA in the biatrial configuration suggests changes are influenced by additional reentrant activity promoted by the RA substrate.

These findings have important implications for computer-based tools informing ablation therapy as the arrhythmia vulnerability ratio is expected to change with RA inclusion. This is especially relevant because successful virtual ablation therapies for AF are based on noninducibility criteria; therefore, performing biatrial simulations seems advisable.

Arrhythmia vulnerability in different remodeling states

The majority of subject models exhibited higher vulnerability in the S state. However, for some, the vulnerability ratio was higher in the M state. To understand this behavior, we analyzed activation patterns of reentries induced only in the M state. In the M state, the fibrotic substrate impeded wavefront propagation, causing unidirectional blocks and anchoring reentries. Conversely, in the S state, increased fibrosis led to slower wavefront progression, facilitating tissue recovery and promoting regular activation. For the other cases in which the S state had a higher vulnerability, the faster wavefront in M encountered refractory tissue and failed to activate the surrounding tissue. However, in the S state, wavefront deceleration and a shortened action potential enabled propagation within the fibrotic region. The overall outcome was a combination of both effects.

Study limitations

To our knowledge, this study represents the first dedicated examination of the role of the RA in arrhythmia vulnerability in patient-specific computer models; however, the limited sample size may impact the generalization of our findings. Different IAC configurations, including varying number, locations, and widths, might affect reentrant pathways. All virtual patient models had a similar fibrosis pattern. CV variation was constrained to 20%. Sustained reentry episodes were simulated for 1 second only. We did not assess changes in structural remodeling concerning endo–epi dissociation, a phenomenon observed in AF patients also in the RA.[30] The absence of electrogram recordings from the study participants prevents the assessment of clinical AF maintenance mechanisms for the simulated reentries.

Conclusion

LA reentry vulnerability in a biatrial model is higher than in a monoatrial model. Incorporating the RA in patient-specific computational models unmasked potential inducing points in the LA. The RA had a substrate-dependent effect on reentry dynamics and affected the TCL of the LA-induced reentries. Because virtual ablation strategies for AF rely on noninducibility criteria, performing biatrial simulations is advisable. Our study highlights the importance of the RA for the maintenance and induction of arrhythmia in patient-specific computational models.

Appendix

Supplementary data

Supplementary data associated with this article can be found in the online version at https://doi.org/10.1016/j.hrthm.2024.01.047.

Funding Sources: This project has received funding from the European Union's Horizon 2020 research and innovation programme under the Marie Skłodowska-Curie Grant Agreement No. 860974. This work was supported by the Leibniz ScienceCampus "Digital Transformation of Research" with funds from the programme "Strategic Networking in the Leibniz Association." The authors acknowledge support by the state of Baden-Württemberg through bwHPC.

Disclosures: The authors have no conflicts to disclose.

Authorship: All authors attest they meet the current ICMJE criteria for authorship.

Address reprint requests and correspondence: Dr Axel Loewe, Institute of Biomedical Engineering, Karlsruhe Institute of Technology (KIT), Fritz-Haber Weg 1 30.33, 76131, Karlsruhe, Germany. E-mail address: publications@ibt.kit.edu

References

1. Haissaguerre N, Hocini M, Sanders P, et al. Localized sources maintaining atrial fibrillation organized by prior ablation. Circulation 2006;113:616–625.
2. Boyle PM, Zghaib T, Zahid S, et al. Computationally guided personalized targeted ablation of persistent atrial fibrillation. Nat Biomed Eng 2019;3:870–879.
3. Azzolin L, Eichenlaub M, Nagel C, et al. Personalized ablation vs. conventional ablation strategies to terminate atrial fibrillation and prevent recurrence. Europace 2023;25:211–222.
4. Lim B, Kim J, Hwang M, et al. In situ procedure for high-efficiency computational modeling of atrial fibrillation reflecting personal anatomy, fiber orientation, fibrosis, and electrophysiology. Sci Rep 2020;10:2417.
5. Roney CH, Sim I, Yu J, et al. Predicting atrial fibrillation recurrence by combining population data and virtual cohorts of patient-specific left atrial models. Circ Arrhythm Electrophysiol 2022;15:e010253–e010253.
6. Krueger MW, Seemann G, Rhode K, et al. Personalization of atrial anatomy and electrophysiology as a basis for clinical modeling of radiofrequency ablation of atrial fibrillation. IEEE Trans Med Imaging 2013;32:73–84.
7. Azzolin L, Eichenlaub M, Nagel C, et al. AugmentA: patient-specific augmented atrial model generation tool. Comput Med Imaging Graph 2023;108:102265.
8. Wachter A, Loewe A, Krueger MW, et al. Mesh structure-independent modeling of patient-specific atrial fiber orientation. Curr Dir Biomed Eng 2015;1:409–412.
9. Courtemanche M, Ramirez RJ, Nattel S. Ionic mechanisms underlying human atrial action potential properties: insights from a mathematical model. Am J Physiol Heart Circ Physiol 1998;275:H301–H321.
10. openCARP Consortium, Augustin C, Boyle PM, Loechner V, et al. Dataset: openCARP (v13.0). May 26, 2023. https://doi.org/10.35097/1027.
11. Plank G, Loewe A, Neic A, et al. The openCARP simulation environment for cardiac electrophysiology. Comput Methods Programs Biomed 2021;208:106223.
12. Martínez Díaz P, Loewe A. Code: The right atrium affects in silico arrhythmia vulnerability in both atria. November 28, 2023. https://doi.org/10.35097/1830.
13. Martínez Díaz P, Sánchez J, Fitzen N, et al. Dataset: the right atrium affects in silico arrhythmia vulnerability in both atria. Zenodo. 2024. https://doi.org/10.5281/zenodo.10724338.
14. Loewe A, Wilhelms M, Dössel O, et al. Influence of chronic atrial fibrillation induced remodeling in a computational electrophysiological model. Biomed Eng 2014;59:S929–S932.
15. Wilhelms M, Hettmann H, Maleckar M, et al. Benchmarking electrophysiological models of human atrial myocytes. Front Physiol 2013;3:1–16.
16. Prabhu S, Voskoboinik A, McLellan A, et al. A comparison of the electrophysiologic and electroanatomic characteristics between the right and left atrium in persistent atrial fibrillation: is the right atrium a window into the left? J Cardiovasc Electrophysiol 2017;28:1109–1116.
17. Loewe A, Krueger MW, Platonov PG, et al. Left and right atrial contribution to the p-wave in realistic computational models. Lecture Notes Comput Sci 2015;9126:439–447.
18. Krueger MW, Dorn A, Keller DUJ, et al. In-silico modeling of atrial repolarization in normal and atrial fibrillation remodeled state. Med Biol Eng Comput 2013;51:1105–1119.
19. Nagel C, Luongo G, Azzolin L, et al. Non-invasive and quantitative estimation of left atrial fibrosis based on P waves of the 12-lead ECG—a large-scale computational study covering anatomical variability. J Clin Med 2021;10:1797.
20. Akoum N, McGann C, Vergara G, et al. Atrial fibrosis quantified using late gadolinium enhancement MRI is associated with sinus node dysfunction requiring pacemaker implant. J Cardiovasc Electrophysiol 2012;23:44–50.
21. Vigmond E, Pashaei A, Amraoui S, et al. Percolation as a mechanism to explain atrial fractionated electrograms and reentry in a fibrosis model based on imaging data. Heart Rhythm 2016;13:1536–1543.
22. Roney CH, Bayer JD, Zahid S, et al. Modelling methodology of atrial fibrosis affects rotor dynamics and electrograms. Europace 2016;18(Suppl 4):iv146–iv155.
23. Azzolin L, Schuler S, Dössel O, et al. A reproducible protocol to assess arrhythmia vulnerability: pacing at the end of the effective refractory period. Front Physiol 2021;12:656411.
24. Nitta T, Imura H, Bessho R, et al. Wavelength and conduction inhomogeneity in each atrium in patients with isolated mitral valve disease and atrial fibrillation. J Cardiovasc Electrophysiol 1999;10:521–528.
25. Hindricks G, Potpara T, Dagres N, et al. 2020 ESC guidelines for the diagnosis and management of atrial fibrillation developed in collaboration with the European Association for Cardio-Thoracic Surgery (EACTS). Eur Heart J 2021;42:373–498.
26. Joglar JA, Chung MK, Armbruster AL, et al. 2023 ACC/AHA/ACCP/HRS guideline for the diagnosis and management of atrial fibrillation: A report of the American College of Cardiology/American Heart Association Joint Committee on Clinical Practice Guidelines. Circulation 2024;149:e1–e156.
27. Roney CH, Williams SE, Cochet H, et al. Patient-specific simulations predict efficacy of ablation of interatrial connections for treatment of persistent atrial fibrillation. Europace 2018;20:iii55–iii68.
28. Zahid S, Cochet H, Boyle PM, et al. Patient-derived models link reentrant driver localization in atrial fibrillation to fibrosis spatial pattern. Cardiovasc Res 2016;110:443–454.
29. Roy A, Varela M, Chubb H, et al. Identifying locations of re-entrant drivers from patient-specific distribution of fibrosis in the left atrium. PLoS Comput Biol 2020;16:e1008086.
30. Kharbanda RK, Knops P, van der Does LJME, et al. Simultaneous endoepicardial mapping of the human right atrium: unraveling atrial excitation. J Am Heart Assoc 2020;17:e017069.